

Development and Degeneration of Retinal Ganglion Cell Axons in *Xenopus tropicalis*

Boyeon Choi^{1,2}, Hyeyoung Kim^{1,2}, Jungim Jang¹, Sihyeon Park¹, and Hosung Jung^{1,*}

¹Department of Anatomy, Graduate School of Medical Science, Brain Korea 21 Project, Yonsei University College of Medicine, Seoul 03722, Korea, ²These authors contributed equally to this work.

*Correspondence: hosungjung@yonsei.ac.kr
<https://doi.org/10.14348/molcells.2022.0081>
www.molcells.org

Neurons make long-distance connections via their axons, and the accuracy and stability of these connections are crucial for brain function. Research using various animal models showed that the molecular and cellular mechanisms underlying the assembly and maintenance of neuronal circuitry are highly conserved in vertebrates. Therefore, to gain a deeper understanding of brain development and maintenance, an efficient vertebrate model is required, where the axons of a defined neuronal cell type can be genetically manipulated and selectively visualized *in vivo*. Placental mammals pose an experimental challenge, as time-consuming breeding of genetically modified animals is required due to their *in utero* development. *Xenopus laevis*, the most commonly used amphibian model, offers comparative advantages, since their embryos *ex utero* during which embryological manipulations can be performed. However, the tetraploidy of the *X. laevis* genome makes them not ideal for genetic studies. Here, we use *Xenopus tropicalis*, a diploid amphibian species, to visualize axonal pathfinding and degeneration of a single central nervous system neuronal cell type, the retinal ganglion cell (RGC). First, we show that RGC axons follow the developmental trajectory previously described in *X. laevis* with a slightly different timeline. Second, we demonstrate that co-electroporation of DNA and/or oligonucleotides enables the visualization of gene function-altered RGC axons in an intact brain. Finally, using this method, we show that the axon-autonomous, Sarm1-dependent axon destruction program operates in *X. tropicalis*. Taken together, the present

study demonstrates that the visual system of *X. tropicalis* is a highly efficient model to identify new molecular mechanisms underlying axon guidance and survival.

Keywords: axon degeneration, axon guidance, development, *Xenopus tropicalis*

INTRODUCTION

The visual system has been a model for many discoveries of the molecular and cellular mechanisms underlying axon guidance (Varadarajan and Huberman, 2018). Retinal ganglion cells (RGCs) are the only projection neurons of the eye, which convey visual information processed in the retina to the visual centers of the brain. RGCs form the inner most layer of the retina, and their axons collect at the optic nerve head (also known as the optic disc) before exiting the eye. Outside the eye, RGC axons form the optic nerve, which enters the brain at the ventral midline of the diencephalon, where the two optic nerves originating from the opposite eyes cross and form the optic chiasm. In vertebrates, most RGC axons terminate at the two visual centers of the brain, the dorsal lateral geniculate nucleus of the thalamus, and the superior colliculus (also known as the optic tectum) of the midbrain. The retinotectal pathway, the collection of RGC axons terminating at the optic tectum, has been used as a key model to study axon guidance (Triplet, 2014), and its development in *Xen-*

Received 13 May, 2022; accepted 15 June, 2022; published online 7 November, 2022

eISSN: 0219-1032

©The Korean Society for Molecular and Cellular Biology.

©This is an open-access article distributed under the terms of the Creative Commons Attribution-NonCommercial-ShareAlike 3.0 Unported License. To view a copy of this license, visit <http://creativecommons.org/licenses/by-nc-sa/3.0/>.

opus laevis, the classic amphibian model, has been described in detail with a particular focus on the temporal relationship between the growth of RGC axons and that of the rest of the body (Erdogan et al., 2016).

All but one species of the genus *Xenopus* are polyploid, and the *X. laevis* belongs to the tetraploid class, hence making it difficult to apply the modern genetic and genomic techniques (Graf and Kobel, 1991). *Xenopus tropicalis* is the only diploid species in the genus *Xenopus* and was recently adopted for research in developmental genetics and genomics (Hirsch et al., 2002). *X. tropicalis* shares the experimental advantages of *X. laevis*, such as the use of classical embryological techniques and the similarity of gross morphology and development to *X. laevis*, suggesting that the knowledge obtained in the studies using *X. laevis* might be applied to *X. tropicalis* (Kakebeen and Wills, 2019). However, whether this assumption holds true in the development of the retinotectal pathway has not been tested.

In the present study, we show the developmental trajectory of RGC axons in *X. tropicalis*. We use two techniques, a Dil-based labeling strategy to visualize all RGC axons navigating the brain, and an electroporation-based strategy to label a few RGC axons in mosaic while simultaneously altering the expression of a specific gene in labeled RGCs. Using these strategies, we report the detailed trajectory of RGC axon growth and guidance at specific developmental stages. Secondly, we present a detailed procedure of the electroporation technique designed specifically for *X. tropicalis* for sparse labeling and visualization of RGC axons *in vivo*. Finally, we use this technique to demonstrate that the axon-autonomous effect of a gene can be efficiently assessed using this system. Specifically, we use Wallerian degeneration, the stereotyped deterioration of a severed axonal fragment (Coleman and Hoke, 2020), as a model and demonstrate that *Wlds* gain-of-function or *Sarm1* loss-of-function delays Wallerian degeneration in an axon-autonomous manner in *X. tropicalis*. Taken

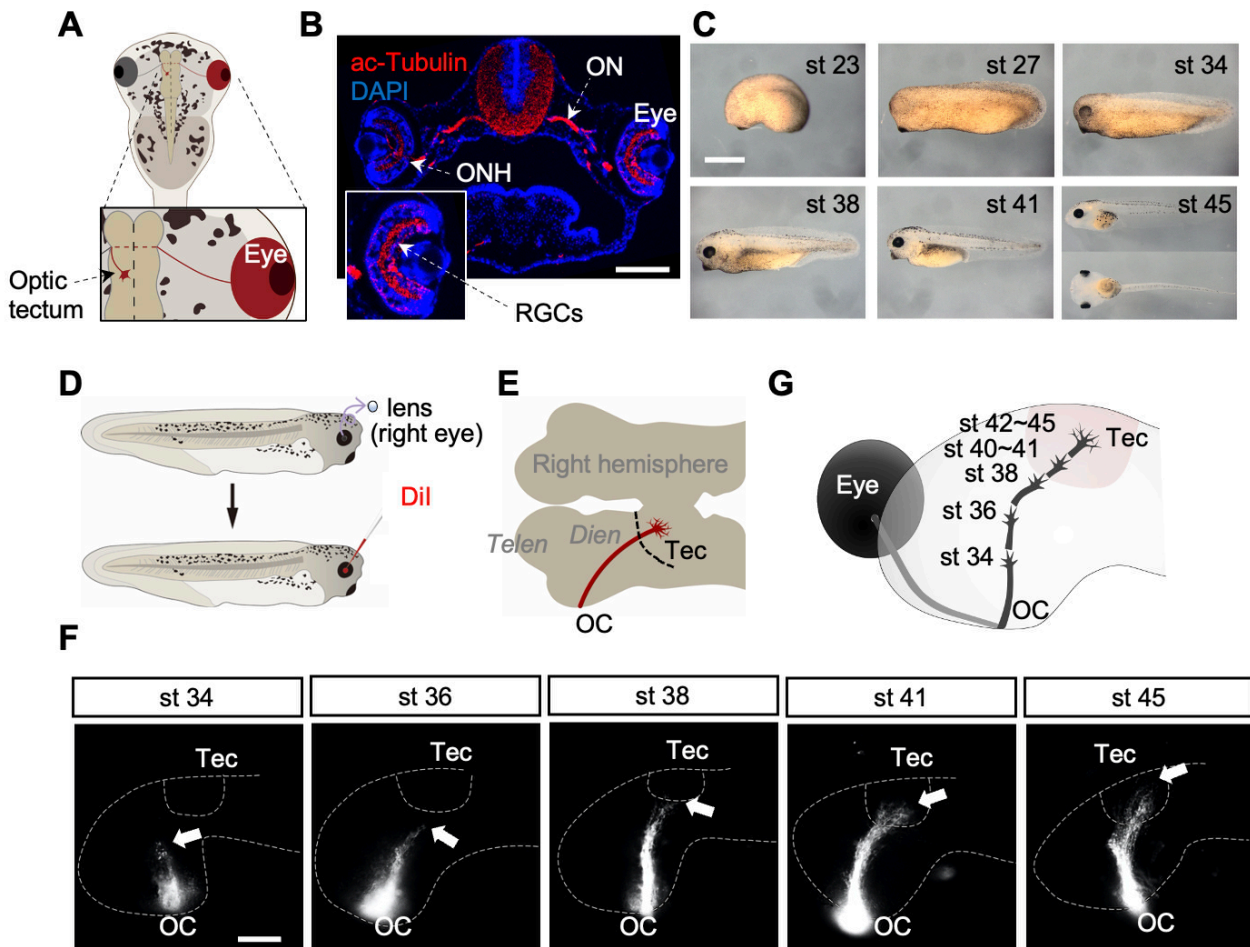


Fig. 1. Development of the retinotectal pathway in *X. tropicalis*. (A) Retinotectal pathway. (B) Coronal section of a stage 45 embryo. Anti-acetylated(ac)-Tubulin immunoreactivity mostly visualizes axons, with nuclear counterstaining (DAPI). ON, optic nerve; ONH, optic nerve head; RGC, retinal ganglion cell. Scale bar = 200 μ m. (C) Photographs of embryos at key developmental stages. st, stage. Scale bar = 1 mm. (D) Dil-labeling of the retinotectal pathway originating from the right eye. (E) "Open book" imaging strategy. OC, optic chiasm; Tec, optic tectum. (F) Dil-labeled retinal axons in the contralateral (left) brain hemisphere viewed from the side. Arrows, the distal tip of the retinotectal pathway. Scale bar = 100 μ m. (G) Summary of retinotectal pathway development in *X. tropicalis*.

together, our study provides a useful framework for future studies to search for new molecular and cellular mechanisms underlying axon guidance and survival, using the embryologically accessible and genetics-friendly model of the retinal axons of *X. tropicalis*.

MATERIALS AND METHODS

Xenopus experiments

X. tropicalis embryos were generated by *in vitro* fertilization, raised in 0.1× modified Barth's saline (MBS) (8.8 mM sodium chloride, 100 μM potassium chloride, 100 μM magnesium sulfate, 500 μM 4-(2-hydroxyethyl)-1-piperazineethanesulfonic acid, 250 μM sodium bicarbonate, and 1 mM calcium chloride) at 21°C–24°C, and staged according to the tables provided in Nieuwkoop and Faber (1967) and Xenbase (<http://www.xenbase.org/>). All experiments complied with the protocols approved by the Yonsei University College of Medicine Institutional Animal Care and Use Committees (No. 2019-0039).

Plasmids and morpholino oligonucleotides

pCMV-tag2B FLAG-WldS was kindly gifted by Professor Michael Coleman (University of Cambridge). Sarm1 anti-sense morpholino (Sarm1 MO), 5'-GAAGAGTGAGAAC-CATGAATCCTTC-3'; and control MO, 5'-ATGGTTTCCA-CAATCTCTCCATCCA-3' conjugated to carboxyfluorescein at the 3' end were purchased from Gene-Tools (USA).

Dil labeling

1,1'-Dioctadecyl-3,3,3'-tetramethylindocarbocyanine perchlorate (Dil; Sigma, USA) crystals were dissolved in chloroform. Embryos were fixed in 4% paraformaldehyde in 1× phosphate buffered saline (PBS) for 2 h at room temperature and immobilized in PBS on a dish containing solidified Sylgard (Sigma). The lens of one eye was removed, and Dil solution was filled into the cavity as shown in Fig. 1D. Dil was allowed to diffuse for approximately 16 h in a humidifying chamber to label RGC axons, after which the brain was dissected out and processed for imaging.

Electroporation

Electroporation was performed based on the method developed for *X. laevis* (Falk et al., 2007), with modifications to account for a smaller size of *X. tropicalis* embryos. Briefly, stage 27–28 embryos were anesthetized with ethyl 3-aminobenzoate methanesulfonate (MS222) in 1× MBS (300 μg/ml). Tadpoles were placed on a custom-made electroporation chamber that was designed to fit a *X. tropicalis* embryo, as shown in Fig. 2A, and two platinum electrodes were placed at the ends of the short axis of the chamber so that the electrical field is placed across the two eyes. Glass pipettes were prepared by pulling heated glass capillary tubes (1.0 mm × 0.78 mm, Harvard apparatus) using a micropipette puller (Sutter P-97). DNA and/or morpholino were dissolved in water to 1–2 μg/ml in total. Approximately 10 nl of solution was microinjected into the ventricular cavity of the optic vesicle near the cathode. The glass pipette was immediately pulled out of the optic vesicle and 1× MBS, after which rectangular

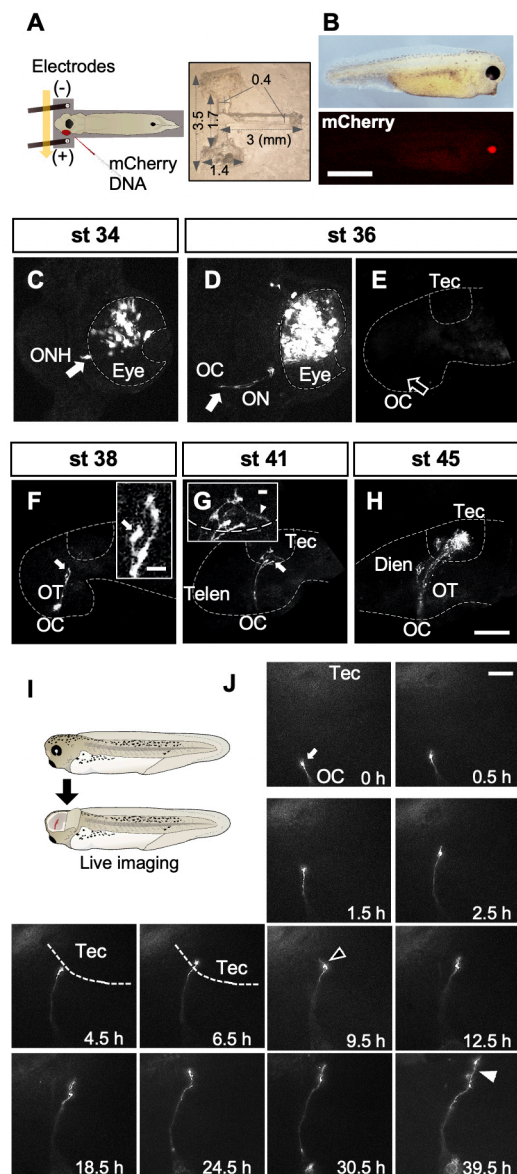


Fig. 2. Visualization of retinotectal pathway development by electroporation. (A) Electroporation of nucleotides into the right retinal primordium by targeted electroporation (left) using a custom-made Sylgard chamber (right). (B) Right eye-specific expression of mCherry encoded in the electroporated plasmid. Scale bar = 1 mm. (C and D) Coronal sections of electroporated right eyes. (E–H) “Open book” visualization of retinal axons growing in or terminating at the contralateral (left) brain hemisphere. st, stage; ONH, optic nerve head; OC, optic chiasm; ON, optic nerve; Tec, optic tectum; OT, optic tract; Telen, telencephalon; Dien, diencephalon; arrows, growth cones at the tip of growing axons; arrowhead, terminal branches of target-arrived axons; hollow arrow, contralateral optic track. Scale bars = 100 μm and 10 μm (inset). (I) Live imaging of electroporated retinal axons growing in an intact brain using “open brain” preparation. (J) Time-lapse photographs of a single retinal axon taken from shortly after midline crossing at the OC for approximately 40 h. Arrows, growth cone; hollow arrowhead, collapsed growth cone; filled arrowhead, extensively branched axon terminal. Scale bar = 50 μm.

pulses were delivered using an electroporator (Intracel TSS20 Ovodyne). Typically, eight consecutive 18 V, 50 ms steps were applied in 1-s intervals. The electroporated embryos were transferred to 0.1× MBS and raised at 21°C–24°C.

Axotomy

After unilateral retinal electroporation of enhanced green fluorescent protein (EGFP)-encoding plasmid, the stage 45 embryos were anesthetized with MS222 in 0.1× MBS, and the electroporated eye was removed. The embryos were transferred to 0.1× MBS and raised at 21°C–24°C for 1–3 days.

Immunofluorescence and cell counting

Fixed embryos were saturated with 30% sucrose in 1× PBS, cryo-sectioned in the coronal plane at the 12- μ m thickness, and mounted on a slide glass. Antigen retrieval was performed in 10 mM sodium citrate with 0.05% Tween-20 (pH 6.0) at 95°C for 20 min. The slides were then blocked in 5% normal donkey serum in 1× PBS-T (0.05% Tween-20 in 1× PBS) for 30 min at room temperature and transferred to the blocking solution containing a rabbit anti-acetylated alpha tubulin antibody (1:300, ab125356; Abcam, UK). After incubating at 4°C for 16 h, the slides were washed three times with PBS-T, and the secondary antibody solution with an anti-rabbit IgG antibody conjugated to Alexa Fluor 555 (A-31572; Sigma) in PBS-T (1:1,000) was added. After incubating at room temperature for 1 h, the slides were washed three times with PBS-T, and nuclei were counterstained with Hoechst 33342 (Sigma) dissolved in 1× PBS (1:20,000). The slides were mounted in FluorSave (Sigma) with a cover glass. Five embryos were randomly chosen per group, and three coronal tissue sections around the longest axis of the eye were selected per embryo for cell counting in Fig. 3.

Imaging

For live imaging of *in vivo* RGC axons, unilaterally electroporated embryos were anesthetized in 300 μ g/ml MS222 in 1× MBS, and the contralateral (un-electroporated) eye, skin, and meninges were removed to expose the contralateral optic tectum. The embryos were then immobilized on a glass-bottom dish in 1.5% low melting agarose dissolved in 300 μ g/ml MS222 in 1× MBS. The dish was then filled with the same solution without agarose, and images were taken at 5-min intervals under an epifluorescence microscope (Eclipse Ti2; Nikon, Japan) equipped with a 20× objective. To image the retina and RGC axons before crossing the midline, the electroporated embryos were fixed in 4% paraformaldehyde dissolved in 1× PBS and cryo-sectioned in the coronal plane. To image RGC axons in the contralateral brain hemisphere, the brains were dissected out of the fixed embryos, the ventral midline was cut open, and the brain was flat-mounted on a slide glass containing 1× PBS with the superior side facing the cover glass, as shown in Fig. 1E. These preparations were imaged under a laser-scanning confocal microscope (LSM 700; Carl Zeiss, Germany) equipped with a 63× C-Apochromat (numerical aperture 1.2) objective.

Software

Images were analyzed using ImageJ (National Institute of

Health, USA). Statistical analyses were performed using R.

RESULTS

Development of the retinotectal pathway in *X. tropicalis*

To systematically assess the developmental stage-dependent growth and pathfinding of RGC axons *in vivo*, we performed a series of time-course experiments. RGC axons exit the eye at the optic nerve head, form a bundle of the optic nerve, and enter the brain at the optic chiasm. In amphibian tadpoles and fish, which lack binocular vision, all RGC axons cross the midline, in contrast to mammals where the temporal RGCs project ipsilaterally. Upon entering the brain, RGC axons travel as a bundle near the superficial layer of the brain forming the optic tract. The RGC axons stay within the optic tract until entering the optic tectum, where they defasciculate and form topographically organized synapses with tectal neurons (Figs. 1A and 1B).

To map the temporal pattern of RGC axon development, we fixed the embryos at different developmental stages (Fig. 1C) and labeled the right retina with Dil (Fig. 1D). The RGC axons originating from the Dil-labeled eye and growing in or terminating at the contralateral (left) brain hemisphere were imaged in a “open-book preparation” (Fig. 1E). We found that the earliest born RGC axons cross the midline prior to stage 34, reach the tectum around stage 38, and enter and arborize in the tectum around stage 41 (Fig. 1F). Up until this stage, late-born RGC axons continue to follow, and the terminal arborization becomes more complex by stage 45. Based on these findings, we found that *X. tropicalis* RGC axon development occurs one or two stages behind when compared to *X. laevis*, and present an updated temporal map of retinotectal pathway development of *X. tropicalis* (Fig. 1G).

Mosaic labeling of retinal axons using unilateral electroporation

Next, we developed an electroporation method to RGC axons in mosaic. We modified the method developed for a much larger *X. laevis* embryo and built the electroporation chamber designed to fit a *X. tropicalis* embryo by making a cross-shaped indentation in a Sylgard dish, in the way that the electrical field can be applied across the two eyes (Fig. 2A). A stage 27 embryo was positioned in the long axis of the indentation on the ventral side up, so that the head and the eyes can be positioned between two electrodes in the short axis of the indentation (Fig. 2A). At this stage, the retina is in the shape of the optic vesicle, an evagination of the neural tube mainly comprised of neural stem cells, of which RGCs are the first-born cells. We injected several nanoliters of solution containing mCherry-encoding plasmids into the ventricle of the optic vesicle facing the cathode, so that the DNA solution diffuse from the center of the optic vesicle. Immediately following the injection, rectangular voltage pulses were delivered so that the negatively charged DNA or fluorescently-tagged morpholino (which by itself is not charged) moves towards the lateral neuroepithelial layer of the optic vesicle facing the cathode.

First, we confirmed that this method targets DNA into the

retina, by imaging the whole embryo (Fig. 2B) or the eviscerated retina in tissue sections (Figs. 2C and 2D). mCherry expression was limited to the retina and not present in the ipsilateral brain, indicating that this protocol selectively labels retinal neuroepithelium (Fig. 2C). Typically, 20%-50% of the retinal cells were targeted slightly biased toward the dorsal retina since the ventral retina forms later as the result of the continued evagination of the neuroepithelium after stage 27 (Holt, 1980), when the electroporation was performed. Using this labeling method, we visualized the axons of electroporated RGCs in the contralateral brain at different developmental stages, with the temporal map constructed in Fig. 1G in mind. We found that the RGC axons labeled in this way were several hours behind the earliest born RGC axons, which we visualized by Dil method (Figs. 2C-2H). For example, we could not see the electroporated RGC axons in the contralateral optic tract in stage 36 (Fig. 2E), whereas Dil-labeled RGC axons reached the diencephalon-mesencephalon border at this stage (Fig. 1F). Likewise, the electroporated RGC axons that

crossed the midline could be visualized only at stage 38 (Fig. 2F), when the Dil-labeled axons already reached the optic tectum (Fig. 1F). This delay is inherent to the electroporation method, as it labels RGCs born at or after stage 27, which is after the birth of the first RGCs around stage 24. However, the developmental trajectory of the electroporated RGC axons were consistent and was of little difference to that of Dil-labeled axons at stage 41 or later, since RGC axons slow down prior to entering the optic tectum (Figs. 2G and 2H).

One advantage of the electroporation over the Dil-based method is that RGC axons are sparsely labeled. Sparse labeling is suitable for imaging individual axons, as evident in clear visualization of the growth cones, the transient structure at the tip of a growing axon, in the optic tract (Fig. 2F, inset), and the terminal axon branches at the optic tectum (Fig. 2G, inset [arrowhead]), which could not be appreciated when all axons were labeled by Dil (Fig. 1F). Second advantage is that it allows live imaging of RGC axons in an intact brain. We visualized the growth of a single RGC axon *in vivo* to see the

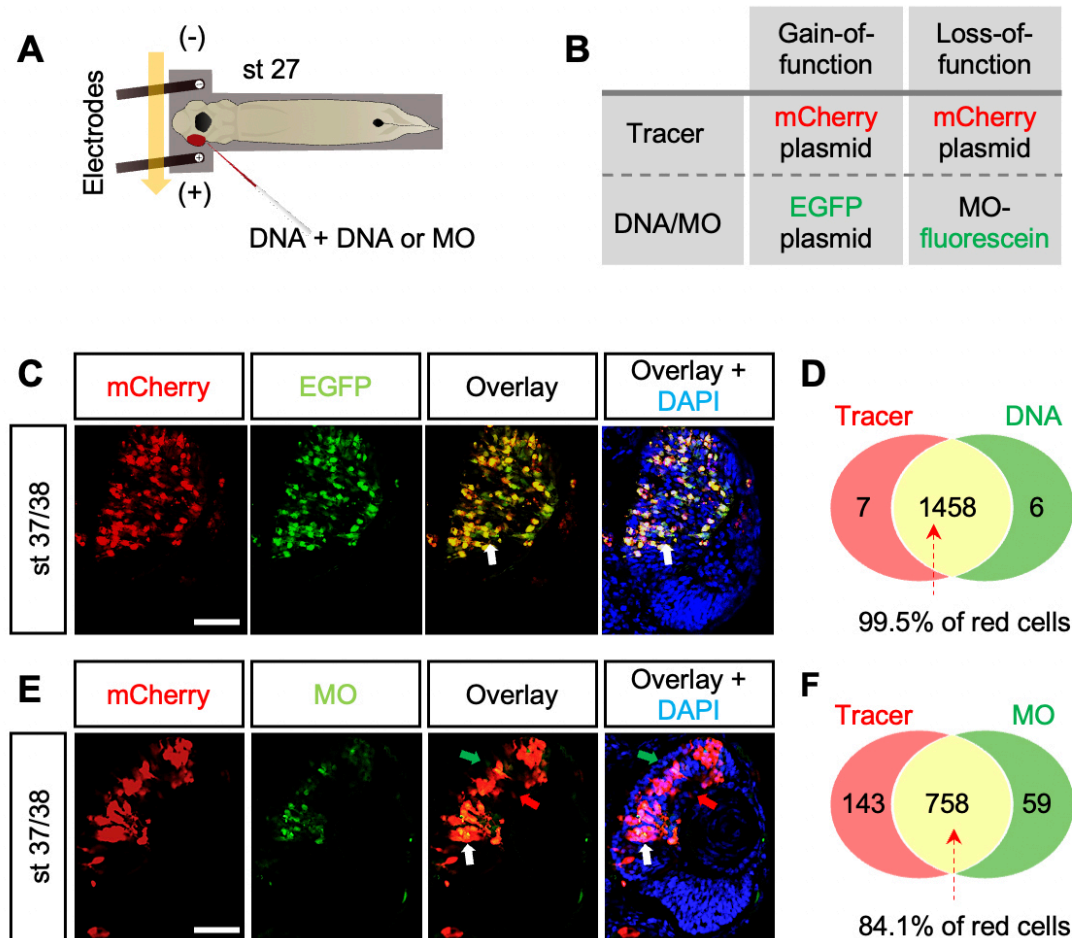


Fig. 3. Assessment of co-electroporation efficiency. (A) mCherry DNA (axon tracer) was mixed with another DNA (EGFP) or fluorescein-tagged morpholino (MO) oligonucleotides, and electroporated into the right retinal primordium. st, stage. (B) Modeling of gain- or loss-of-function by co-electroporation of DNA or MO with a tracer. (C and D) Coronal section (C) of the retina after DNA-DNA co-electroporation and cell counting (D). Scale bar = 50 μ m. (E and F) Coronal section (E) of the retina after DNA-MO co-electroporation and cell counting (F). Scale bar = 50 μ m. White arrows, overlay; Green arrows, fluorescein-tagged antisense morpholino (MO); Red arrows, mCherry.

rapid growth of a growth cone-tipped axon from the optic chiasm to the optic tectum (Figs. 2I and 2F, arrow), which took place in approximately 6 h, pausing of the growth cone at the tectal entry site, and breaking down of the growth cone and subsequent axon branching at the tectum (Fig. 2J, arrowhead) that occurs over days (Fig. 2J, Supplementary Movie S1). Therefore, the electroporation method described here can be used to label RGCs in mosaic and to visualize their axons growing in the contralateral brain.

Co-electroporation strategy of gain- and loss-of-function approaches

The final, and perhaps the most important, advantage of the electroporation over the Dil method is that gene expression of the RGC whose axons will be visualized can be selectively manipulated without altering the rest of the body by co-electroporating gene expression or function-altering reagent along with an axon tracer (Fig. 3A). For example, gain- or loss-of-function studies can be performed by co-electroporating a protein-coding plasmid or an anti-sense oligonucleotide with an mCherry-encoding plasmid as a tracer (Fig. 3B). Implicit in this approach is that mCherry-expressing axons always contain the co-electroporated molecules. We assessed this possibility by measuring the co-electroporation efficiency of mCherry and EGFP plasmids or mCherry and fluorescein-tagged antisense morpholino (MO), synthetic nucleotides that inhibit the translation of target mRNAs by steric hindrance of ribosome binding. After co-electroporation of a tracer plasmid (mCherry) together with a gain-of-function plasmid (EGFP) or a loss-of-function oligonucleotide (MO-fluorescein) at stage 27, we visualized the progeny of electroporated cells (i.e., mCherry-positive cells) in the retina at stage 37/38. We asked how many of mCherry-positive cells co-inherit EGFP or MO-fluorescein, by counting green and/or red cells in retinal sections. We found that over 99% and 84% of mCherry-positive cells were positive for EGFP (Figs. 3C and 3D) and MO-fluorescein (Figs. 3E and 3F), respectively. As fluorescence of the MO-fluorescein molecules does not amplify in contrast to the fluorescence originating from the EGFP-encoding plasmid, our co-electroporation efficacy of DNA-MO is likely to be an underestimation. Therefore, imaging mCherry-positive axons in the contralateral optic tectum after co-electroporation gives a reasonably high chance of imaging retinal axons, in which the function and/or expression of a specific gene is altered, in an otherwise wild-type brain.

Wlds-protectable and *Sarm1*-dependent axon destruction program operates in *X. tropicalis*

Wallerian degeneration is a sequence of stereotypical events leading to disintegration of the distal axonal fragment separated from the cell body (Coleman and Hoke, 2020). Recently, an exciting series of research demonstrated that Wallerian degeneration proceeds as a result of the active axon destruction program, whose components converge on the biochemical pathway that generates and consumes NAD^+ . For example, *Nmnat2*, an enzyme responsible for the rate-limiting step in the NAD^+ biogenesis, is required for axon survival, and its gain-of-function by *Wlds* protects severed axons from Wallerian degeneration for weeks, a naturally oc-

curing *NMNAT* mutant protein in mouse, which re-routes its enzymatic activity to ectopic subcellular localizations (Mack et al., 2001). Surprisingly, *Wlds* delays Wallerian degeneration even in fly, suggesting not only that an evolutionarily conserved mechanism regulates a programmed destruction of axonal fragments, but also that a forward genetic screening strategy can be applied to discover new genes that regulate axon destruction. In this approach, *dSarm* (Drosophila homolog of mammalian *Sarm1*), the gene with the exact opposite effect, was identified, and the loss-of-function in *Sarm1* delayed Wallerian degeneration both in mouse and fly (Osterloh et al., 2012). Intriguingly, *Sarm1* displayed an unexpected NADase activity that directly counteracts *Nmnat2*, positioning the NAD^+ metabolism at the center of the axon destruction program. However, it remains unclear how the NAD^+ metabolism regulates axon survival and destruction, and it is necessary to identify new genes and pathways that participate in the axon destruction program.

Based on the results of our co-electroporation study, we reasoned that the visual system of *X. tropicalis* is a good system to search for such genes, as the axon-autonomous effect of a gene can be directly visualized *in vivo* by co-electroporating. As a proof-of-concept, we constructed RGC-specific *Wlds* gain-of-function and *Sarm1* loss-of-function models. We first established the time-course of Wallerian degeneration of wild-type retinal axons. After electroporation of EGFP-encoding plasmid at stage 27, the electroporated retina was separated from the optic nerve at stage 45 (Fig. 4A), when the most RGC axons form stably synapses with tectal neurons (Fig. 4B), and visualized distal axonal fragments following axotomy (Figs. 4C–4F). We could visualize highly reproducible morphological features of Wallerian degeneration *in vivo*, and fragmented axons were clearly visible in 24 h post axotomy (Fig. 4D). Most axonal fragments were cleared in 48 h post-axotomy (Fig. 4E), and no traces of axons were visible in 72 h (Fig. 4F). The beaded morphology of degenerating axons, a key feature of Wallerian degeneration, became most evident in 48 h post-axotomy (Figs. 4G and 4H), and we used this time point for the remainder of our experiments.

Then, we co-electroporated a *Wlds*-encoding plasmid or a *Sarm1* antisense MO with EGFP-encoding plasmid (as an axon tracer) and asked whether these manipulations protect axons from Wallerian degeneration. We imaged severed axons 48 h post-axotomy, when most wild-type axons degenerate (Figs. 5A and 5B). Strikingly, co-electroporating the *Wlds*-encoding plasmid prevented Wallerian degeneration in all animals tested (Figs. 5C and 5D), indicating that *Wlds* gain-of-function suppresses the axon destruction program in *Xenopus*. *Sarm1* loss-of-function also protected axons, although we did not observe the protective effect in approximately 20% of the cases (Figs. 5E and 5F). Since MO electroporation-based loss-of-function approach inhibits the synthesis of *Sarm1*, without removing pre-existing *Sarm1* proteins, the relatively weaker effect of the *Sarm1* MO compared with the *Wlds*-plasmid may be ascribed to the function of *Sarm1* proteins synthesized before MO delivery. It also might have resulted from a relatively lower (~84%) co-electroporation efficacy of DNA-MO compared to that of DNA-DNA co-electroporation (~99%) (Figs. 3D and 3F). Nonetheless, com-

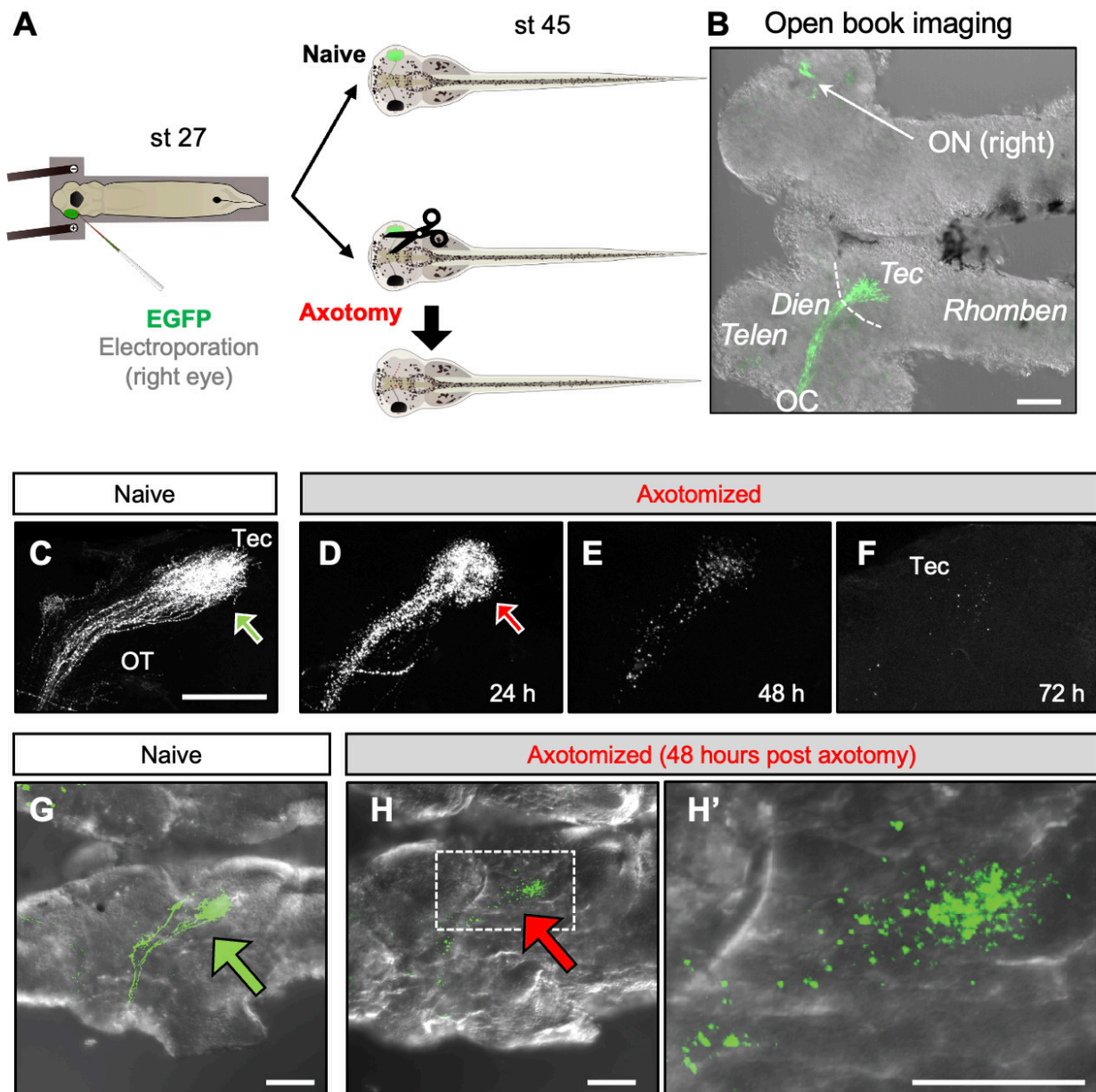


Fig. 4. Wallerian degeneration of retinal axons *in vivo*. (A) Strategy to visualize Wallerian degeneration of retinal axons. st, stage. (B) Open book imaging of electroporated, fully mature retinal axons. Telen, telencephalon; Dien, diencephalon; Tec, optic tectum; Rhomben, rhombencephalon; ON, optic nerve; OC, optic chiasm. Scale bar = 100 μ m. (C-F) Time-course of Wallerian degeneration of retinal axons *in vivo*. Green and red arrows indicate healthy and degenerating axons, respectively. OT, optic tract. Scale bar = 100 μ m. (G and H) Retinal axon before (G) and 48 h after axotomy (H and H'). Green and red arrows indicate healthy and degenerating axons, respectively. Note the beaded morphology of degenerating axons. Scale bars = 100 μ m.

pared to the wild-type axons, none of which survived axotomy, Sarm1 MO electroporation delayed Wallerian degeneration in nearly 80% of cases. Taken together, our results show that the axon destruction program operates in *Xenopus*, as described in mouse and fly, and suggest that the selective visualization of gene function-altered axons in wild-type brain is a promising strategy to search for new genes involved in the axon destruction program.

DISCUSSION

The present study demonstrates the first detailed temporal map of retinotectal pathway development in *X. tropicalis*. Using this map, we developed a co-electroporation-based approach for mosaic visualization of retinal axons, in which the function of a specific gene can be manipulated, in a wild-type embryo. We also map the temporal pattern of retinal axon growth and arborization labeled in this way and show,

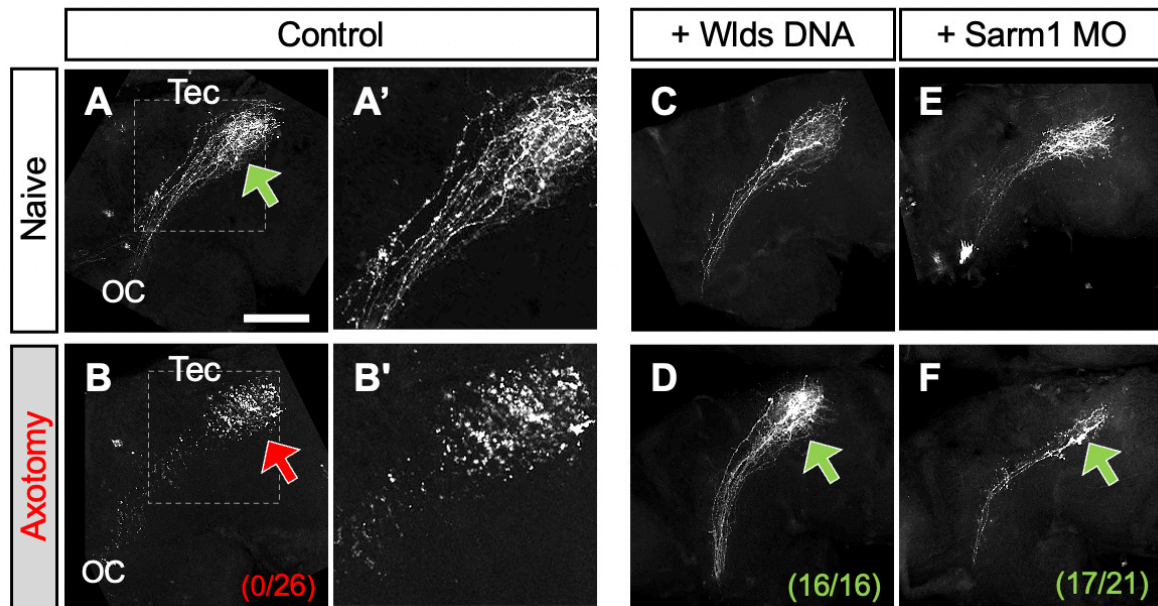


Fig. 5. Axon-autonomous function of Wlds and Sarm1 in Wallerian degeneration. The same experiments were performed as described in Fig. 4, except that Wlds-encoding plasmid or Sarm1 translation-blocking antisense morpholino (MO) oligonucleotide was co-electroporated with mCherry tracer. (A and B) Control axons without gene alteration. Axotomy induces near-synchronous degeneration of distal axons (red arrow) in all animals tested (0/26). A' and B' are enlarged image of the boxed area in A and B, respectively. Red and green arrows indicate degenerating and healthy axons, respectively. OC, optic chiasm; Tec, optic tectum. (C and D) Wlds protects severed axons from degeneration in all animals tested (green arrow, 16/16). $P = 6.0 \times 10^{-12}$, Fisher's exact test versus control. (E and F) Sarm1 MO protects severed axons in 81% of animals tested (green arrow, 17/21). $P = 2.2 \times 10^{-9}$, Fisher's exact test versus control. Scale bar = 100 μm .

as a proof of concept, that the axon destruction pathway can be suppressed by Wlds gain-of-function and Sarm1 loss-of-function in an axon-autonomous manner.

The retinotectal pathway in *X. laevis* has been an invaluable model to study the molecular and cellular mechanisms underlying axon guidance (van Horck et al., 2004), topographic map formation (Mann et al., 2002) and axon survival (Yoon et al., 2012). However, the allotetraploid genome of *X. laevis* poses challenges in applying genetic approaches, and the diploid *X. tropicalis* has slowly been adopted to overcome this limitation (Kakebeen and Wills, 2019). Most genes in the *X. laevis* genome contain two homeologs, and both genes must be targeted, for example, by using a mixture of two guide RNAs in the Crispr/Cas9 system, to obtain a knockout embryo (Wang et al., 2015), whereas a single gene targeting can be used in *X. tropicalis* (Guo et al., 2014). The developmental processes of the retinotectal pathway in *X. tropicalis* and the experimental strategies to specifically visualize electroporated RGC axons *in vivo* described in the present study make it possible to utilize both classic knowledge gained in the studies of *X. laevis* and the advantage of the modern *X. tropicalis* model.

Recent studies have clearly shown that axon degeneration is run by the active axon destruction pathway, which is conceptually similar to but molecularly different from the programmed cell death. The genes that promote or inhibit the axon destruction program has been identified, key molecules being Sarm1 and Nmnat2, respectively (Coleman and Hoke, 2020). Additional players of this pathway are being actively searched for, although the progress is not as rapid as hoped.

One potential difficulty might be gene redundancy of vertebrates, which may cause loss-of-function-based screenings fail to find a phenotype-altering gene. For example, *Drosophila axundead (axed)* is required for Wallerian degeneration to proceed downstream of Sarm1, suggesting that it is an executor of axon degeneration after injury (Neukomm et al., 2017) that is inhibited during developmental axon branching (Izadifar et al., 2021). However, it has not been determined whether this also operates in vertebrates, mainly since there are four putative vertebrate paralogs. Unlike genetic approaches that involve generation of quadruple knockout animals, the electroporation-based mosaic approach could provide a potentially efficient tool to simultaneously knock-out or knock-down multiple genes and examine the loss-of-function phenotype in F0 generation. Likewise, genetic screenings to search for the genes regulating axon guidance could also be performed efficiently, as a library of guide RNAs for Crispr/Cas9 can also electroporated into one eye, and the embryos with axon pathfinding defects can be screened in F0 generation, by comparing their axonal trajectories with the reference map presented here. Together, the information and techniques presented in this study provide a useful reference for future studies of axon development and degeneration.

Note: Supplementary information is available on the Molecules and Cells website (www.molcells.org).

ACKNOWLEDGMENTS

This work was supported by Samsung Science and Tech-

nology Foundation (SSTF-BA1602-13) and the National Research Foundation of Korea (NRF) grants funded by the Korean government (MSIT) (2013M3A9D5072551, 2017R1A2B4002683, and 2018R1A5A2025079) to H.J.

AUTHOR CONTRIBUTIONS

B.C., H.K., J.J., and S.P. performed experiments. H.J. wrote the manuscript with the help of all authors.

CONFLICT OF INTEREST

The authors have no potential conflicts of interest to disclose.

ORCID

Boyoon Choi <https://orcid.org/0000-0002-1068-6013>
Hyeyoung Kim <https://orcid.org/0000-0003-3129-9650>
Jungim Jang <https://orcid.org/0000-0003-0832-7422>
Sihyeon Park <https://orcid.org/0000-0003-0425-8036>
Hosung Jung <https://orcid.org/0000-0002-5059-8050>

REFERENCES

- Coleman, M.P. and Hoke, A. (2020). Programmed axon degeneration: from mouse to mechanism to medicine. *Nat. Rev. Neurosci.* *21*, 183-196.
- Erdogan, B., Ebbert, P.T., and Lowery, L.A. (2016). Using *Xenopus laevis* retinal and spinal neurons to study mechanisms of axon guidance in vivo and in vitro. *Semin. Cell Dev. Biol.* *51*, 64-72.
- Falk, J., Drinjakovic, J., Leung, K.M., Dwivedy, A., Regan, A.G., Piper, M., and Holt, C.E. (2007). Electroporation of cDNA/Morpholinos to targeted areas of embryonic CNS in *Xenopus*. *BMC Dev. Biol.* *7*, 107.
- Graf, J.D. and Kobel, H.R. (1991). Genetics of *Xenopus laevis*. *Methods Cell Biol.* *36*, 19-34.
- Guo, X., Zhang, T., Hu, Z., Zhang, Y., Shi, Z., Wang, Q., Cui, Y., Wang, F., Zhao, H., and Chen, Y. (2014). Efficient RNA/Cas9-mediated genome editing in *Xenopus tropicalis*. *Development* *141*, 707-714.
- Hirsch, N., Zimmerman, L.B., and Grainger, R.M. (2002). *Xenopus*, the next generation: *X. tropicalis* genetics and genomics. *Dev. Dyn.* *225*, 422-433.
- Holt, C. (1980). Cell movements in *Xenopus* eye development. *Nature* *287*, 850-852.
- Izadifar, A., Courchet, J., Virga, D.M., Verreet, T., Hamilton, S., Ayaz, D., Misbaer, A., Vandenbogaerde, S., Monteiro, L., Petrovic, M., et al. (2021). Axon morphogenesis and maintenance require an evolutionary conserved safeguard function of Wnk kinases antagonizing Sarm and Axed. *Neuron* *109*, 2864-2883.e8.
- Takebe, A. and Wills, A. (2019). Advancing genetic and genomic technologies deepen the pool for discovery in *Xenopus tropicalis*. *Dev. Dyn.* *248*, 620-625.
- Mack, T.G., Reiner, M., Beirowski, B., Mi, W., Emanuelli, M., Wagner, D., Thomson, D., Gillingwater, T., Court, F., Conforti, L., et al. (2001). Wallerian degeneration of injured axons and synapses is delayed by a Ube4b/Nmnat chimeric gene. *Nat. Neurosci.* *4*, 1199-1206.
- Mann, F., Ray, S., Harris, W., and Holt, C. (2002). Topographic mapping in dorsoventral axis of the *Xenopus* retinotectal system depends on signaling through ephrin-B ligands. *Neuron* *35*, 461-473.
- Neukomm, L.J., Burdett, T.C., Seeds, A.M., Hampel, S., Coutinho-Budd, J.C., Farley, J.E., Wong, J., Karadeniz, Y.B., Osterloh, J.M., Sheehan, A.E., et al. (2017). Axon death pathways converge on Axundead to promote functional and structural axon disassembly. *Neuron* *95*, 78-91.e5.
- Nieuwkoop, P.D. and Faber, J. (1967). *Normal Table of Xenopus Laevis (Daudin): A Systematical and Chronological Survey of the Development from the Fertilized Egg Till the End of Metamorphosis (2nd Edition)* (Amsterdam: North-Holland Publishing Company).
- Osterloh, J.M., Yang, J., Rooney, T.M., Fox, A.N., Adalbert, R., Powell, E.H., Sheehan, A.E., Avery, M.A., Hackett, R., Logan, M.A., et al. (2012). dSarm/Sarm1 is required for activation of an injury-induced axon death pathway. *Science* *337*, 481-484.
- Triplet, J.W. (2014). Molecular guidance of retinotopic map development in the midbrain. *Curr. Opin. Neurobiol.* *24*, 7-12.
- van Horck, F.P., Weinl, C., and Holt, C.E. (2004). Retinal axon guidance: novel mechanisms for steering. *Curr. Opin. Neurobiol.* *14*, 61-66.
- Varadarajan, S.G. and Huberman, A.D. (2018). Assembly and repair of eye-to-brain connections. *Curr. Opin. Neurobiol.* *53*, 198-209.
- Wang, F., Shi, Z., Cui, Y., Guo, X., Shi, Y.B., and Chen, Y. (2015). Targeted gene disruption in *Xenopus laevis* using CRISPR/Cas9. *Cell Biosci.* *5*, 15.
- Yoon, B.C., Jung, H., Dwivedy, A., O'Hare, C.M., Zivraj, K.H., and Holt, C.E. (2012). Local translation of extranuclear lamin B promotes axon maintenance. *Cell* *148*, 752-764.